

# Task state decoding and mapping of individual four-dimensional fMRI time series using deep neural network

Xiaoxiao Wang<sup>1#\*</sup>, Xiao Liang<sup>1#</sup>, Yawen Zhou<sup>1</sup>, Yanming Wang<sup>1</sup>, Jin Cui<sup>1</sup>, Huijuan Wang<sup>1</sup>, Yu Li<sup>1</sup>, Benedictor Alexander Nguchu<sup>1</sup>, Bensheng Qiu<sup>1,2\*</sup>

1 Centers for Biomedical Engineering, University of Science and Technology of China, Hefei, China.

2 Anhui Computer Application institute of Traditional Chinese Medicine, Hefei, China

# These authors contribute equally.

## \* Correspondence:

Bensheng Qiu

[bqiu@ustc.edu.cn](mailto:bqiu@ustc.edu.cn)

Xiaoxiao Wang

[wang506@ustc.edu.cn](mailto:wang506@ustc.edu.cn)

## Abstract

Decoding specific task states from human fMRI (functional magnetic resonance imaging) signals constitutes a major goal of neuroimaging. Previous studies of task-state classification have focused largely on processed fMRI characteristics (e.g. functional connectivity patterns, activity patterns) or a single fMRI volume. Here, we assembled a novel deep neural network (DNN) for classifying directly from 4-D fMRI time series, retaining both spatial and temporal information of fMRI signals. We trained and tested the DNN classifier by task fMRI data from human connectome project (HCP) S1200 dataset. Reading just a single block of fMRI time series of each task for each individual, the novel classification method identified the seven tasks with 91.75% accuracy in test. Then we extracted task heatmaps of each time series by a guided backpropagation approach, and found that the heatmaps had a high similarity with the group average result of traditional contrast of parameter estimate (COPE). Furthermore, the DNN could be applied to small dataset. The features from the intermediate layer of the DNN were trained and used to train a support vector machine (SVM) to classify four conditions within 300 blocks of task-fMRI scans, data amount comparable to a usual neuroimaging research, and obtained a 95% accuracy. Our reported findings were the first to demonstrate the ability of DNN to classify and extract heatmaps from a 4-D fMRI time series, as well as its ability to be transfer trained by a small dataset. This approach should enable decoding and mapping subject's task status and furthermore help with classification and diagnosis of neuropsychiatric diseases.

## Keywords

brain decoding, deep learning, functional magnetic resonance imaging, fMRI, transfer learning, functional brain mapping

## **Abbreviations**

AMSI – activation map similarity indices

AUC – area under curve

BN – batch normalization

BOLD – blood-oxygen-level dependent

CNN – convolutional neural network

COPE – contrast of parameter estimate

CT – computed tomography

DBN – deep belief network

DL – deep learning

DNN – deep neural network

FEAT – FMRIB's Expert Analysis Tool

fMRI – functional magnetic resonance imaging

FSL – FMRIB Software Library

HCP – human connectome project

HRF – haemodynamic response function

M1 – primary motor cortex

M2 – secondary motor cortex

MNI – Montreal Neurological Institute

MVPA – multi-voxel pattern analysis

RBM – restricted Boltzmann machine

ReLU – rectified linear unit

ROC – receiver operating characteristics

S1 – primary somatosensory area

SGD – stochastic gradient descent

SVM – support vector machine

WM – working memory

## 1 Introduction

For years, researchers have been trying to decode and distinguish task states from functional brain imaging data. Approaches have focused on decoding motor state from cortical activity (Dehaene et al., 1998); inferring internal cognitive states with whole-brain connectivity patterns (Shirer et al., 2012); selecting arbitrary objects with linear regressed patterns of voxels' signal (Horikawa and Kamitani, 2017); and classifying task state from voxels within a single fMRI volume (Jang et al., 2017). To our knowledge, all previous classification studies have not directly analyzed the 4-D blood-oxygen-level dependent (BOLD) fMRI signals, which contain the most temporal and spatial information of the brain activity, thus these classification methods lose more or less spatiotemporal information within the fMRI signals. Therefore, it is of interest to propose a classifier directly on the 4-D fMRI time series.

The BOLD fMRI data is relatively a massive data problem, data obtained in a single fMRI scan (5–20 minutes) contain  $10^8$  sampling points (hundred thousand in one brain volume and hundreds volumes in a scan), which are hard to analyze directly. Hence, neuroimaging researchers have generally chosen to employ general linear model (GLM) to extract task-specific features (Worsley and Friston, 1995) or Pearson-correlation to obtain brain functional connectivity (Biswal et al., 1995), so as the neuroimaging classification researchers (Chadwick et al., 2010; Plis et al., 2014; Shirer et al., 2012). With linear assumptions, these approaches dramatically reduced data size into a single volume or a correlation matrix, but obscured the dynamical and nonlinear characteristics of the BOLD (Friston et al., 1998). In recent years, deep neural networks (DNN) were developed and showed great performance in dealing with massive data (LeCun et al., 2015). The hierarchical structure of DNN with nonlinear activation function can learn more complex output function than traditional machine learning methods and can be trained end-to-end. DNN can also extract high level features from the raw input data while these feature have been demonstrated to have a better representation ability than hand-crafted features (Sharif Razavian et al., 2014). Deep learning (DL) has already yielded remarkable results in structural MRI analysis, such as multi-modality isointense infant brain image segmentation (Zhang et al., 2015) and brain tumor segmentation (Havaei et al., 2017). Taking together, these findings indicated the possibility of applying DNN for classification of 4-D fMRI time series.

The application of DL in neuroimaging is limited by the massive acquirement of data samples for the DL. The usual quantity of data in a typical neuroimaging study is around tens of subjects, while training of a DL needs at least tens of thousands of samples. Collecting massive samples is not suitable for most of the researches, since it is quite costly and time-consuming. Besides, some situations or patients are limited, and data are not easily collected (Litjens et al., 2017). Recently, a number of methods have been proposed to train DNN on limited medical data, and one of the most widely applied ones is the transfer learning (Sharif Razavian et al., 2014). Ciompi et al. (2015) trained the output layer of a natural image classification deep model OverFeat (Sermanet et al., 2013) for the classifying computed tomography (CT) scans. However, different from the traditional visual task like objection detection or segmentation that can use the deep models pre-trained by numerous natural images, it is infeasible to apply the pre-trained models to neuroimaging data directly due to

most of neuroimaging data having different modalities and data structures from natural images. Recent big fMRI projects such as HCP (Van Essen et al., 2013) and BioBank (Miller et al., 2016) give us a chance to access to massive fMRI data. Thus, it is now practically possible to train a DNN directly from big fMRI data, and generalize for small fMRI researches.

In this study, we proposed a DNN classifier that could classify 4-D individual task fMRI signals. The DNN was trained, validated and tested with imaging data downloaded from the HCP S1200 task-fMRI dataset. Then we extracted task heatmaps from each time series by a guided backpropagation approach, and evaluated their similarity with the group average Cohen's d effect. Finally, an SVM with the features that extracted from the intermediate layer of our trained model was employed to classify new tasks, and we found that, with the trained feature extractors, the SVM could learn and identify new task states from data of the order of usual neuroimaging research.

## 2 Methods

### 2.1 HCP

Here we used the dataset from the Human Connectome Project (HCP) S1200 minimal preprocessed 3T data release, which collected imaging and behavioral data from a large population of young healthy adults (Van Essen et al., 2013). 1034 participants of the HCP, who performed all the seven tasks, were included in the recent study. The seven tasks are emotion, gambling, language, motor, relational, social, and working memory (WM), during which a wide range of brain cortex excellently activated (Barch et al., 2013). Further details about the recruitment process, imaging data acquisition, behavior collections and MRI preprocessing can be found in Barch et al. (2013); Van Essen et al. (2013); and Van Essen et al. (2012).

### 2.2 Preparation of fMRI time series for deep learning

Task	Selected Condition	Duration of the Block (seconds)
Emotion	Fear	18
Gambling	Loss	28
Language	Present Story	20
Motor	Right Hand	12
Relational	Relation	16
Social	Mental	23
Working Memory (WM)	2-back places	27.5

**Table 1. Details of the selected BOLD time series for each task.**

We analyzed the HCP volume-based preprocessed fMRI data, which have been already normalized to the Montreal Neurological Institute (MNI) 152 space, and masked with the brain mask (Glasser et al., 2013). A single condition for each task of the subject was selected, and the details were listed in the Table 1. For each condition, the extracted BOLD series are the ones covering the whole block and 8 seconds post the block for including of the post signal of haemodynamic response function

(HRF). And we furtherly cropped out the empty regions, so the input data vary from  $27 \times 75 \times 93 \times 81$  to  $50 \times 75 \times 93 \times 81$  (TR=0.72 secs). A total of 7238 fMRI 4-D data (i.e. 1 4-D data/run  $\times$  1 run/task  $\times$  7 tasks/subject  $\times$  1034 subjects) were included across all tasks and all subjects.

### 2.3 Data augmentation

Big data plays an important role in training deep neural networks. Despite the huge success of deep neural networks, it was still a problem to apply deep neural networks to limited data. Data augmentation as an efficient way to generate more samples, and have been widely used in real world application. The main purpose of data augmentation was to increase the variations of data, which can prevent overfitting and improve the invariance of neural networks. Different from traditional image, all of the input data in the experiment had already been aligned to the standard MNI152 space, so it seemed to be redundant to do data augmentation in spatial domain. Considering of the varied time lengths of the input data, in order to improve the generalization ability of the neural networks to this situation, we randomly sampled  $k$  ( $k=27$  in our experiments) sequential time slices from the data in training phases, and only the first  $k$  sequential time slices were selected in validating and testing phases.

### 2.4 DNN

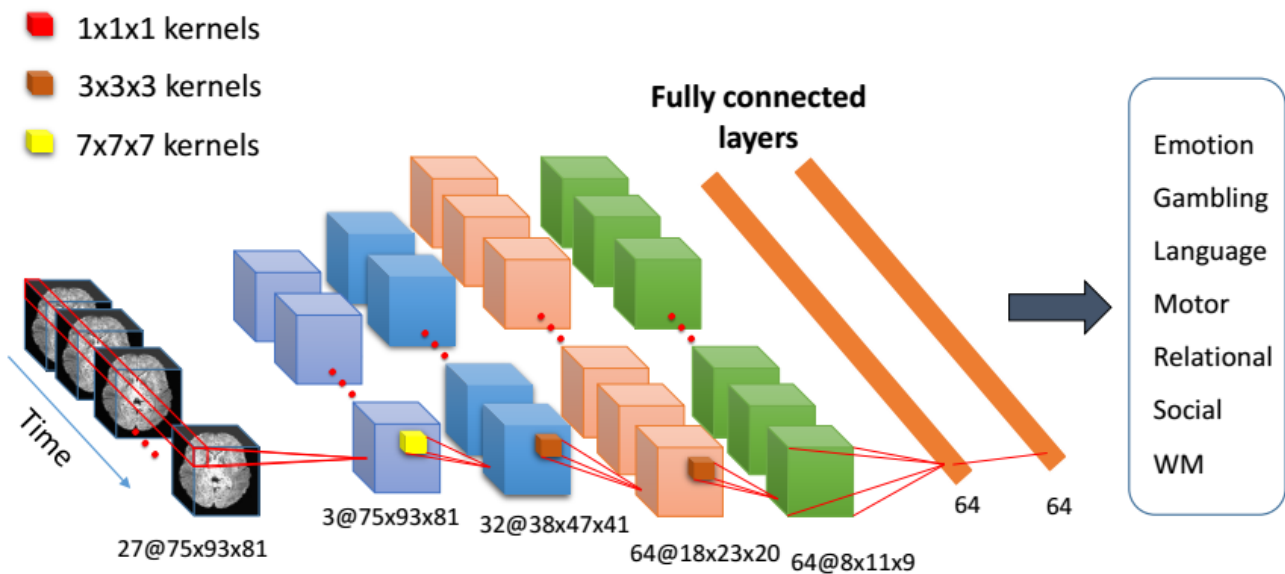


**Figure 1. Overview of our proposed network.** The network consists of five convolutional layers and two fully-connected layers. We take fMRI scans as model input and their labeled task classes as output.

Figure 1 illustrated a flow diagram of our proposed network, which consisted of five convolutional layers and two fully-connected layers. In our experiments, a  $27 \times 75 \times 93 \times 81$  data was generated via previous preprocessing and data augment steps. We used  $1 \times 1 \times 1$  convolutional filters in the first layer, of which kind has been widely used in present structural design of convolutional neural networks for its property of increasing the non-linearity without changing the receptive fields of the

convolutional layer (Hu et al., 2017; Iandola et al., 2016; Simonyan and Zisserman, 2014). The 1x1x1 convolution generated a descriptor for every voxel in fMRI volume over time and the weights of filter were learnable during training, and thus we reduced the samples in time dimension from 27 into three effectively. We adopted stride 2 in all remaining three 3x3x3 or 7x7x7 convolutional layers, and these layers tended to reduce their dimensionality quickly via large size of filters. Instead of pooling operation in the last convolutional layer, we used the fully convolution which could be treated as fully-connected layer. Two fully-connected layers were adopted after a stack of convolutional layers, with the first one had 64 channels, and the other one performed 7-way classification (one for each class). In our models, rectified linear unit (ReLU) function (Krizhevsky et al., 2012) and batch normalization (BN) layer (Ioffe and Szegedy, 2015) were applied after each convolutional layer, while the softmax function was employed in last fully-connected layer.

The implementation of our proposed network has based on PyTorch framework (<https://github.com/pytorch/pytorch>). The network was trained from scratch and all the weights were initialized as He et al. (2015). To guarantee effectiveness, a stochastic gradient descent (SGD) method ran with initial learning rate 0.003 decreasing to 0.001 after 11 epochs. Due to the constraint of memory of the graphic board, the batch size was set to 16. A weight decay of 0.0001 and a momentum of 0.9 was used. The entire dataset was split into training (70%), validation (10%), test (20%) sets. To prevent overfitting training was stopped after 37 epochs.

## 2.5 Transfer learning

An important advantage of the Deep Learning methods, CNN in particular, compared with traditional methods, was the reusability, meaning that trained CNN could be directly used on the similar tasks. In order to validate our model for general use, new tasks were assigned to the trained model. We collect 300 samples with four different new tasks - left hand movement, left foot movement, right foot movement, and tongue movement. All the data were preprocessed as described by the scheme. The data were randomly split into two parts, 80% for training and the rest for testing. After feeding the model with data, the outputs from the fourth layer were treated as features that generate 50688-dimension feature vectors, each representing characteristics of its corresponding respective filed. A sparse SVM classifier was employed after extracting the feature for each sample. The L1-norm regularization was employed to get the sparse solutions.

## 2.6 Analysis

The guided backpropagation (Springenberg et al., 2014) was applied to produce heatmaps of each classification and task-weight representations of the input fMRI 4-D time series. After feeding the trained networks with data, 27 x 75x93x81 prediction gradients were produced in respect to input data. Then, the signed value with absolute maximum in time domain for each voxel was drawn out and built up a 3-D task heatmap, which was then normalized to the absolute maximum of the volume. By interpretation, the voxel with higher heatmap value represents higher voxel-task correlation, contrary to the remaining voxels. In addition, the Cohen's D effects of normalized heatmaps of the test group were calculated as the mean of the individual subject (lev2) heatmaps, divided by the standard deviation (st.d.) of the individual subject heatmaps (Cohen, 2013). To have a

comparison between the traditional GLM map and the heatmap, we get the COPE with HCP standard task analysis pipeline's (Glasser et al., 2013) fsf file with FSL FEAT (FMRIB's Expert Analysis Tool, Smith et al. (2004)).

Activation map similarity indices (AMSI) were calculated to evaluate how perfectly the activated brain areas matched the 'gold standard' activation map. Specifically, a binary mask for each participant was created from surface nodes with effect values at highest  $h$  percentile ( $h=5\%$  and  $10\%$  in the present work). In addition, a binary 'gold standard' mask for each task was created from surface nodes for group average Cohen's D effect at highest percentile levels  $h$ . Subsequently, the Jaccard similarity index of each mask and the 'gold standard' mask was computed across participants, resulting in AMSIs at each percentile level. Here, the computation of Index is based on calculating the ratio of number of overlapping activated voxels to the total number of district voxels.

### 3 Results

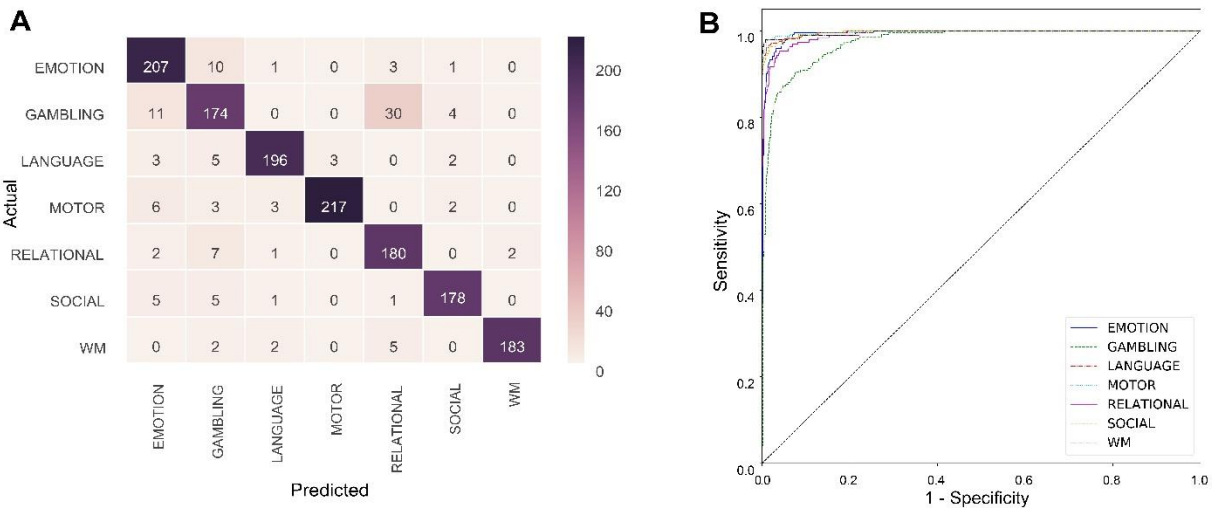


**Figure 2. Counts of predicted label for each task (A), and the classification ROC curve of the proposed model (B).**

To avoid overfitting problem, we used early-stopping and stopped the training after the 37th epoch, at which point the proposed model was found to successfully distinguish seven tasks at an accuracy of 91.75%. As shown in Figure 2A, an analysis of classification indicated that the classifier performed best in WM labeling (accuracy=95.31%) and performed worst in gambling labeling (accuracy=79.45%). The training session cost about 48 hours for the 37 epochs on a NVIDIA GTX 1080 board. Figure 2B illustrated the receiver operating characteristics (ROC) curves, in which motor is found to have largest area under curve (AUC=0.9974) while gambling possess the smallest area (AUC=0.9744).

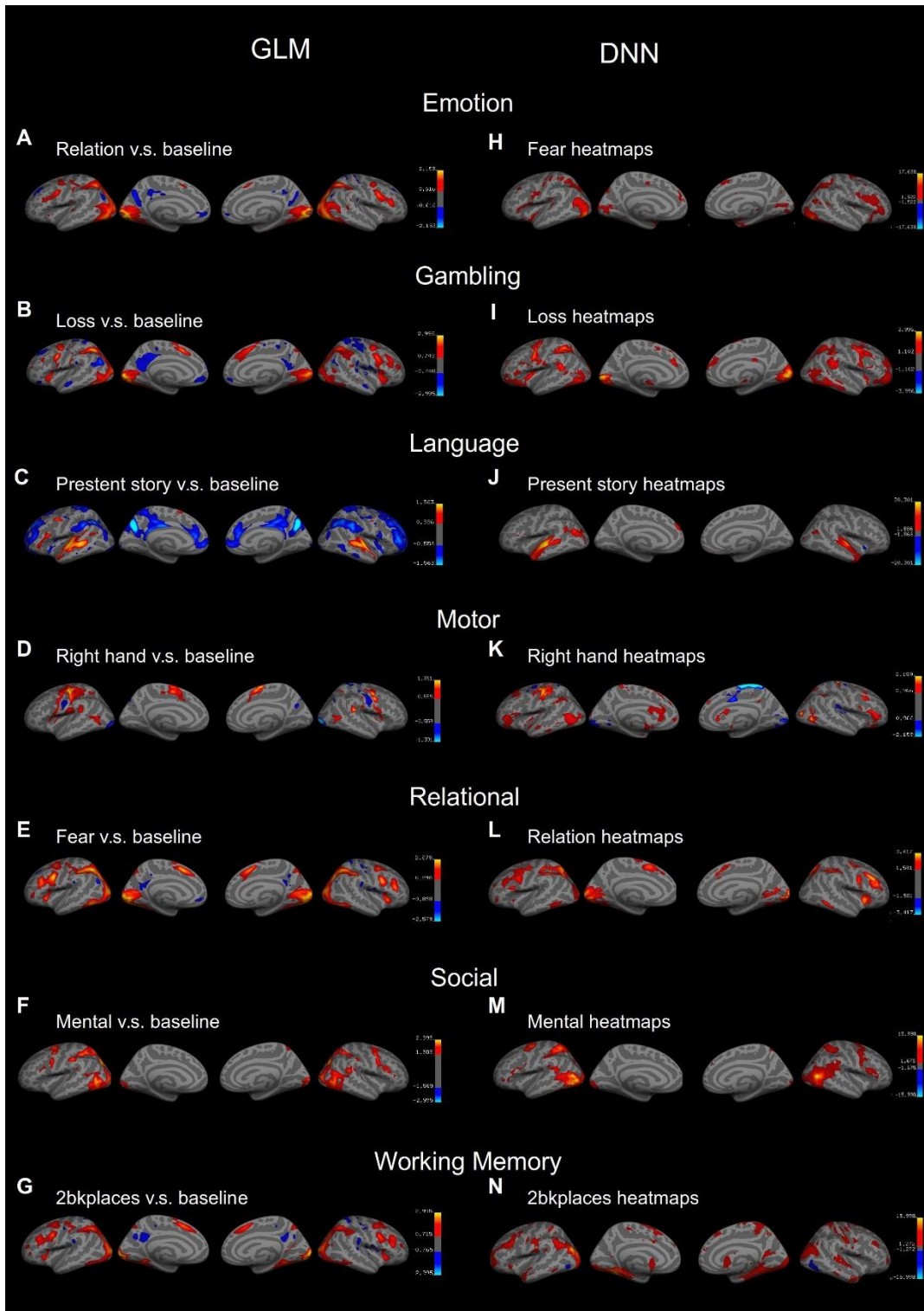


**Figure 3. Cohen's d effect of HCP group average (left column) and of DNN heatmaps (right column) of HCP S1200 dataset.**

In order to visualize features learned by our model, we produced heatmaps by using guided backpropagation (Springenberg et al., 2014). Figure 3 showed group statistical maps for the Cohen's d effect of GLM analysis of task contrast of parameter estimate (COPE, Figure 3 left column), as well as Cohen's d effect of DNN's heatmaps (Figure 3 right column). As the figure illustrated, the

Cohen's d effects of DNN's heatmaps were similar with those of GLM COPEs across all the seven task conditions. For example, both maps showed activity in ventral lateral prefrontal cortex and in both superior and inferior temporal cortices in story presentation condition (Figure 3C and 3J) of the language task. Moreover, both maps revealed similar activity in left primary motor cortex (M1), primary somatosensory area (S1), secondary motor cortex (M2) and bilateral anterior occipital sulcus in right hand movement condition (Figure 4D and 4K) of the motor task.

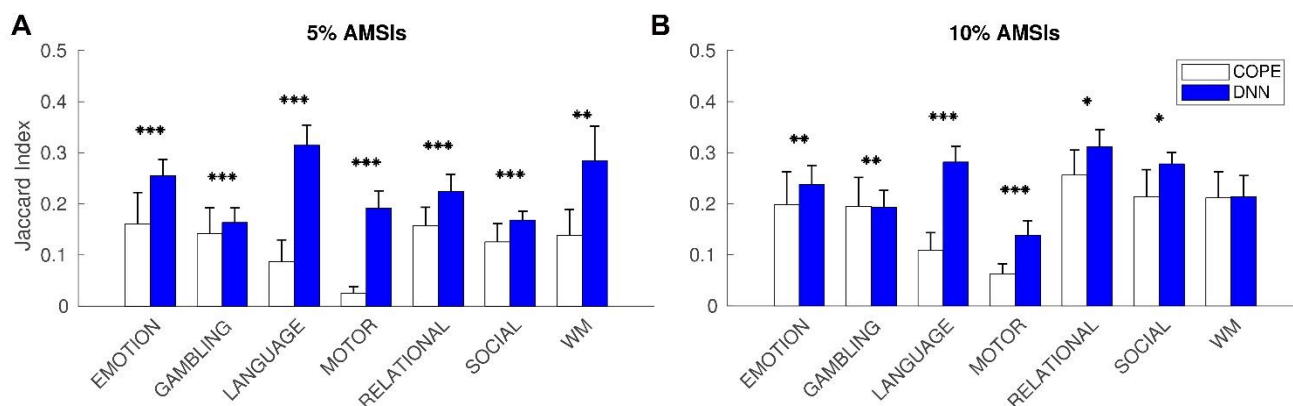


**Figure 4. AMSIs between HCP group average with COPEs (white bars) and with the DNN heatmaps (blue bars).** \* p<0.05, \*\* p<1e-3, \*\*\* p<1e-6 (uncorrected), error bars indicating standard deviation (st.d.)

The spatial correspondence between the activation maps of the two groups was characterized by the AMSI. AMSI would be lower for the group with less overlapping voxels, i.e. group with more spatial variability in activation, with the HCP Cohen's d group average result. Analyzing COPEs for massive data is time consuming, so we only randomly selected 296 scans out of 1455 scans of the test group. Then we compared the AMSIs of COPEs and AMSIs of DNN heatmaps, and the results showed that DNN heatmaps had significantly higher AMSIs than COPEs' in both the percentile levels (Figure 4), indicating that DNN activation heatmaps were more similar with group average activity maps.

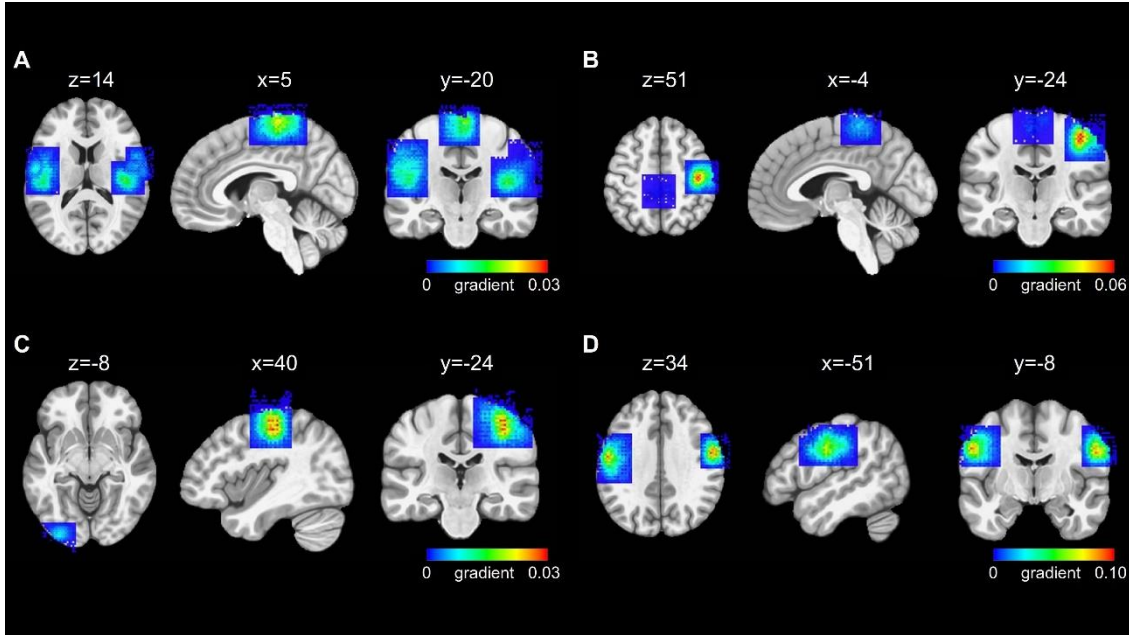


**Figure 5. The non-zero gradient features in SVM classifiers in left foot movement (A, 20 features), right foot movement (B, 13 features), left hand movement (C, 15 features), and tongue movement (D, 4 features).**

Finally, we employed the fourth layer outputs of the DNN as the features for a new classification task. After training and sparsity of the SVM classifier, the classification accuracy reached 95%. This result demonstrated that our model had the ability to encode fMRI BOLD signals for distinguishing new tasks. More interestingly, we visualized the features employed by the sparse SVM for classification and found that only very few of the all 50688 features in M1, M2, S1, and the primary visual cortex were employed (Figure 5).

#### 4 Discussion

In this study, we presented the utility of the deep neural network for the classification of a 4-D fMRI time series. Moreover, the DNN was further trained for the classification of fMRI time series obtained from the seven HCP tasks. The classification accuracies were evaluated across all the seven tasks, and got up to 91.75%. We then drew classification heatmaps and found that short time DNN heatmaps had a higher similarity coefficient with the Group average responses than the traditional full scan GLM drawn COPEs. Then we found that the SVM with DNN features could be trained by a comparable data size in a typical neuroimaging experiment. The proposed DNN method was efficient in classifying and drawing up features of different tasks in a short 4-D fMRI scan, valuable to both research and clinical applications.

The fMRI study of the human brain has historically been led by relating brain activation to designed internal mental state or designated tasks. In conventional task fMRI data analysis, an observed response of the neural system was modeled by the model-based general linear model (GLM, Worsley and Friston (1995)). However, researchers found that the nonlinear components of the responses were shown to be statistically significant (Friston et al., 1998; Miller et al., 2001), and this could be

due to trial-trial interactions (Friston et al., 1998), saturation of the BOLD signal (Miller et al., 2001), stimuli-internal brain activity interactions (He, 2013), and spatiotemporal hemodynamic responses (Aquino et al., 2014). Machine learning methods are good at abstracting information from high-dimensional data space and have been widely appreciated in multivoxel/multivariate pattern analysis (Kriegeskorte et al., 2006; Murphy et al., 2017). Furthermore, the DL has been described as a potentially more powerful approach than conventional shallow machine learning, as it is capable of learning highly intricate and abstract patterns from the data, which can be particularly useful in the case of brain-based disorders (Plis et al., 2014). Prior studies have classified brain BOLD activity by artificial neural networks. In Jang et al. (2017), the authors classified fMRI volumes between four overt sensorimotor tasks, and extracted task-specific features. They made an fMRI volume into a 1-D vector as inputs and found among other results that a three layer CNN could classify the fMRI volumes in minimum error rates. Recent proof (Kim et al., 2016) of using the DNN analysis of whole-brain functional connectivity enabled the classification between schizophrenic patients and normal controls. Plis et al. (2014) proposed a deep belief network (DBN) in conjunction with restricted Boltzmann machine (RBM) that could reveal physiologically important representations in schizophrenia and Huntington disease neuroimaging data. These previous studies usually used fully-connected layer as their basic building block of models, and could not capture spatiotemporal information as good as the proposed CNN. In the present work, we adopted CNN into learning of 4-D fMRI time series, and the classification performances were shown in figure 2A&2B. The classification performance varied across different task states, which could not be explained by the data augment, for task WM and task gambling had comparable block duration (Table 1) but obviously different accuracies. The mislabels on gambling data were mainly relational (Figure 2A), which activated similar brain areas with gambling task (Figure 3B&3E). Thus, a potential explanation for low accuracy in classification of gambling task might be its similarity with the relational tasks, which needed a further investigation.

We have also extracted task specific features with the help of CNN, concurrent the previous feature extraction work (Jang et al., 2017), in which a ROI-wise activity weight maps of nodes in output layer were extracted as the specific features. The idea of applying machine learning to characterizing functional brain regions is not new. Multi-voxel pattern analysis (MVPA) has already been widely used in fMRI data analysis (Norman et al., 2006). For example, by whole-brain MVPA searchlight analysis, Huffman and Stark (2017) have found that human brain context and item representations were influenced by low-level stimulus features. Researchers have also employed multi-layer DNNs to investigate the function of the human sensory system (Yamins and DiCarlo, 2016), such as explicit gradients for feature complexity align the ventral pathway of the human brain (Guclu and van Gerven, 2015), human visual cortical activity maps elicited by visual stimulations (Eickenberg et al., 2017). For a thorough comparison, we also performed experiments with traditional GLM methods in the present work. We assessed the AMSIs of CNN and traditional GLM methods with the group average as the "gold standard". Our present work further got voxel-wise activity maps, which, as shown in the results, outperformed the wide-used GLM method even from a shorter data time series (one block vs. full scan) in similarity index with HCP group average result. This advantage might be due to our preservation of both spatial and temporal nonlinear information of the BOLD time series while performing CNN.

The application of DL in neuroimaging is limited by the sample size, which is usually of hundreds in research and is small compared with other DL applications (e.g. ImageNet contains more than 1 million annotated images, Deng 2009). Researchers have presented various strategies to solve the problem. One of the most widely applied strategy is the transfer learning (Sharif Razavian et al., 2014). For example, Ciompi et al. (2015) employed a deep model OverFeat (Sermanet et al., 2013) trained over numerous natural images and then trained its output layer with CT scans. However, referring to the 4-D fMRI data, the models were needed to be redesigned or retrained because of the lack of large available 4-D natural image datasets or public trained 4-D models. Our method provide a way to be trained with big fMRI dataset to get the features and to apply the features to the classification of small data size. The transfer learned tasks in present work were the tongue, left hand, left foot and right foot motoring tasks that were similar to while different with the pre-trained right hand motor data, all of which were influenced more by features in S1, M1 and M2 than features in other cortical areas (Figure 3K and Figure 5). Moreover, careful examination of the Figure 3K and Figure 5 revealed that the subcortical feature preferences were different, that each classification of motoring body parts preferred more to features in their classical cortical homunculus representations (Penfield and Boldrey, 1937), suggesting re-weights of features during SVM training. The benefits of transfer learning are positively related to the similarity between the data of pre-training and training (Yosinski et al., 2014). The seven tasks employed in the HCP S1200 task-fMRI dataset as a whole provided excellent brain activation coverage (Barch et al., 2013), thus the classifier we proposed could be potential for brain-state decoding from fMRI data of usual sample size of a wide range of tasks.

The present results could be improved in at least two directions. First, using scene could be improved through ability of processing event-related fMRI scan, which was block design only in the present study. As researchers have already demonstrated, the block design obtains more power, while the event-related design obtains a finer characterization of the BOLD activity (Liu et al., 2001), less subject's expectation effects (D'Esposito et al., 1999), less sensitive to head motion (Birn et al., 1999), and more comparable with other trial-based neuroscientific methods (Josephs and Henson, 1999), and is widely used in neuroimaging researches. BOLD activity in a typical event-related design responses simultaneously to several timing-nearby trials, and could be treated as a multi-label classification problem in machine learning, and thus an artificial neural network with multi-label classifier (Yeh et al., 2017) could be applicable to event-related fMRI time series. Second, current method still had some limitations in processing temporal information. Models such as recurrent neural network or convolutional LSTM (Long Short-Term Memory) network are able to process the data with varying length sequences and more appropriate for the time series forecasting problems, and may have a better performance while dealing with the temporal information in fMRI.

Our approach allowed the decoding of the subject's task state from a short 4-D fMRI scan. This new method may provide a basis for a brain-based information retrieval system by classifying brain activity into different categories (e.g. "normal" vs. "abnormal"). This reading may be beneficial for real-time fMRI neurofeedback (Sulzer et al., 2013), as well as brain-based disorder or psychiatry classification (Vieira et al., 2017). Presurgical fMRI has been used for presurgical localization of different motor, somatosensory, as well as language areas, while the paradigm suffered mostly from

long examination time induced patient compliance problems (Tyndall et al., 2017). The proposed method also offered clinicians with the opportunity of extracting task related features from a short 4-D fMRI scan (less than 30 seconds). How well the proposed method could improve the presurgical localization needed a further study.

Overall, our method was the first to classify and extract task-related information directly from 4-D fMRI time series. The presented method can: 1. classify a label of <30s fMRI scan among the 7 typical behavior tasks; 2. learn the task-related brain activity heatmap; 3. transfer learn a new classification with amount of fMRI data that could be obtained in a typical task-fMRI research. The present study likely had wide implications for both neuroscience researches and clinical applications.

## **5 Conflict of Interest**

The authors declare that the research was conducted in the absence of any commercial or financial relationships that could be construed as a potential conflict of interest.

## **6 Acknowledgement**

The author(s) disclose receipt of the following financial support for the research, authorship, and/or publication of this article: this study was supported by the National Natural Science Foundation of China (91432301 and 81701665) and by the Fundamental Research Funds for the Central Universities of China (WK2070000033).

## **7 Reference**

- Aquino, K.M., Robinson, P.A., Drysdale, P.M., 2014. Spatiotemporal hemodynamic response functions derived from physiology. *J. Theor. Biol.* 347, 118-136, doi:10.1016/j.jtbi.2013.12.027.
- Barch, D.M., Burgess, G.C., Harms, M.P., Petersen, S.E., Schlaggar, B.L., Corbetta, M., Glasser, M.F., Curtiss, S., Dixit, S., Feldt, C., Nolan, D., Bryant, E., Hartley, T., Footer, O., Bjork, J.M., Poldrack, R., Smith, S., Johansen-Berg, H., Snyder, A.Z., Van Essen, D.C., Consortium, W.U.-M.H., 2013. Function in the human connectome: task-fMRI and individual differences in behavior. *NeuroImage* 80, 169-189, doi:10.1016/j.neuroimage.2013.05.033.
- Birn, R.M., Bandettini, P.A., Cox, R.W., Shaker, R., 1999. Event-related fMRI of tasks involving brief motion. *Hum. Brain Mapp.* 7, 106-114, doi:10.1002/(SICI)1097-0193(1999)7:2<106::AID-HBM4>3.0.CO;2-O.
- Biswal, B., Yetkin, F.Z., Haughton, V.M., Hyde, J.S., 1995. Functional connectivity in the motor cortex of resting human brain using echo-planar MRI. *Magn. Reson. Med.* 34, 537-541, doi:10.1002/mrm.1910340409.
- Chadwick, M.J., Hassabis, D., Weiskopf, N., Maguire, E.A., 2010. Decoding individual episodic memory traces in the human hippocampus. *Curr. Biol.* 20, 544-547, doi:10.1016/j.cub.2010.01.053.
- Ciampi, F., de Hoop, B., van Riel, S.J., Chung, K., Scholten, E.T., Oudkerk, M., de Jong, P.A., Prokop, M., van Ginneken, B., 2015. Automatic classification of pulmonary peri-fissural nodules in

computed tomography using an ensemble of 2D views and a convolutional neural network out-of-the-box. *Med. Image Anal.* 26, 195-202, doi:10.1016/j.media.2015.08.001.

Cohen, J., 2013. *Statistical Power Analysis for the Behavioral Sciences*. Second edition. Taylor & Francis.

D'Esposito, M., Zarahn, E., Aguirre, G.K., 1999. Event-related functional MRI: implications for cognitive psychology. *Psychol. Bull.* 125, 155-164, doi:10.1037/0033-2909.125.1.155.

Dehaene, S., Le Clec, H.G., Cohen, L., Poline, J.B., van de Moortele, P.F., Le Bihan, D., 1998. Inferring behavior from functional brain images. *Nat. Neurosci.* 1, 549-550, doi:10.1038/2785.

Eickenberg, M., Gramfort, A., Varoquaux, G., Thirion, B., 2017. Seeing it all: Convolutional network layers map the function of the human visual system. *NeuroImage* 152, 184-194, doi:10.1016/j.neuroimage.2016.10.001.

Friston, K.J., Josephs, O., Rees, G., Turner, R., 1998. Nonlinear event-related responses in fMRI. *Magn. Reson. Med.* 39, 41-52, doi:10.1002/mrm.1910390109.

Glasser, M.F., Sotiropoulos, S.N., Wilson, J.A., Coalson, T.S., Fischl, B., Andersson, J.L., Xu, J., Jbabdi, S., Webster, M., Polimeni, J.R., Van Essen, D.C., Jenkinson, M., Consortium, W.U.-M.H., 2013. The minimal preprocessing pipelines for the Human Connectome Project. *NeuroImage* 80, 105-124, doi:10.1016/j.neuroimage.2013.04.127.

Guclu, U., van Gerven, M.A., 2015. Deep Neural Networks Reveal a Gradient in the Complexity of Neural Representations across the Ventral Stream. *J. Neurosci.* 35, 10005-10014, doi:10.1523/JNEUROSCI.5023-14.2015.

Havaei, M., Davy, A., Warde-Farley, D., Biard, A., Courville, A., Bengio, Y., Pal, C., Jodoin, P.M., Larochelle, H., 2017. Brain tumor segmentation with Deep Neural Networks. *Med. Image Anal.* 35, 18-31, doi:10.1016/j.media.2016.05.004.

He, B.J., 2013. Spontaneous and task-evoked brain activity negatively interact. *J. Neurosci.* 33, 4672-4682, doi:10.1523/JNEUROSCI.2922-12.2013.

He, K.M., Zhang, X.Y., Ren, S.Q., Sun, J., 2015. Delving Deep into Rectifiers: Surpassing Human-Level Performance on ImageNet Classification. 2015 Ieee International Conference on Computer Vision (Iccv), 1026-1034, doi:10.1109/Iccv.2015.123.

Horikawa, T., Kamitani, Y., 2017. Generic decoding of seen and imagined objects using hierarchical visual features. *Nat Commun* 8, 15037, doi:10.1038/ncomms15037.

Hu, J., Shen, L., Sun, G., 2017. Squeeze-and-excitation networks. arXiv preprint arXiv:1709.01507.

Huffman, D.J., Stark, C.E.L., 2017. The influence of low-level stimulus features on the representation of contexts, items, and their mnemonic associations. *NeuroImage* 155, 513-529, doi:10.1016/j.neuroimage.2017.04.019.

Iandola, F.N., Han, S., Moskewicz, M.W., Ashraf, K., Dally, W.J., Keutzer, K., 2016. SqueezeNet: AlexNet-level accuracy with 50x fewer parameters and < 0.5 MB model size. arXiv preprint arXiv:1602.07360.

- Ioffe, S., Szegedy, C., 2015. Batch normalization: Accelerating deep network training by reducing internal covariate shift. *International Conference on Machine Learning*, pp. 448-456.
- Jang, H., Plis, S.M., Calhoun, V.D., Lee, J.H., 2017. Task-specific feature extraction and classification of fMRI volumes using a deep neural network initialized with a deep belief network: Evaluation using sensorimotor tasks. *NeuroImage* 145, 314-328, doi:10.1016/j.neuroimage.2016.04.003.
- Josephs, O., Henson, R.N., 1999. Event-related functional magnetic resonance imaging: modelling, inference and optimization. *Philos. Trans. R. Soc. Lond. B Biol. Sci.* 354, 1215-1228, doi:10.1098/rstb.1999.0475.
- Kim, J., Calhoun, V.D., Shim, E., Lee, J.H., 2016. Deep neural network with weight sparsity control and pre-training extracts hierarchical features and enhances classification performance: Evidence from whole-brain resting-state functional connectivity patterns of schizophrenia. *NeuroImage* 124, 127-146, doi:10.1016/j.neuroimage.2015.05.018.
- Kriegeskorte, N., Goebel, R., Bandettini, P., 2006. Information-based functional brain mapping. *Proc. Natl. Acad. Sci. U. S. A.* 103, 3863-3868, doi:10.1073/pnas.0600244103.
- Krizhevsky, A., Sutskever, I., Hinton, G.E., 2012. Imagenet classification with deep convolutional neural networks. *Adv. Neural Inf. Process. Syst.*, pp. 1097-1105.
- LeCun, Y., Bengio, Y., Hinton, G., 2015. Deep learning. *Nature* 521, 436-444, doi:10.1038/nature14539.
- Litjens, G., Kooi, T., Bejnordi, B.E., Setio, A.A.A., Ciompi, F., Ghafoorian, M., van der Laak, J., van Ginneken, B., Sanchez, C.I., 2017. A survey on deep learning in medical image analysis. *Med. Image Anal.* 42, 60-88, doi:10.1016/j.media.2017.07.005.
- Liu, T.T., Frank, L.R., Wong, E.C., Buxton, R.B., 2001. Detection power, estimation efficiency, and predictability in event-related fMRI. *NeuroImage* 13, 759-773, doi:10.1006/nimg.2000.0728.
- Miller, K.L., Alfaro-Almagro, F., Bangerter, N.K., Thomas, D.L., Yacoub, E., Xu, J., Bartsch, A.J., Jbabdi, S., Sotiropoulos, S.N., Andersson, J.L., Griffanti, L., Douaud, G., Okell, T.W., Weale, P., Dragonu, I., Garratt, S., Hudson, S., Collins, R., Jenkinson, M., Matthews, P.M., Smith, S.M., 2016. Multimodal population brain imaging in the UK Biobank prospective epidemiological study. *Nat. Neurosci.* 19, 1523-1536, doi:10.1038/nn.4393.
- Miller, K.L., Luh, W.M., Liu, T.T., Martinez, A., Obata, T., Wong, E.C., Frank, L.R., Buxton, R.B., 2001. Nonlinear temporal dynamics of the cerebral blood flow response. *Hum. Brain Mapp.* 13, 1-12, doi:10.1002/hbm.1020.
- Murphy, C., Rueschemeyer, S.A., Watson, D., Karapanagiotidis, T., Smallwood, J., Jefferies, E., 2017. Fractionating the anterior temporal lobe: MVPA reveals differential responses to input and conceptual modality. *NeuroImage* 147, 19-31, doi:10.1016/j.neuroimage.2016.11.067.
- Norman, K.A., Polyn, S.M., Detre, G.J., Haxby, J.V., 2006. Beyond mind-reading: multi-voxel pattern analysis of fMRI data. *Trends Cogn. Sci.* 10, 424-430, doi:10.1016/j.tics.2006.07.005.

Penfield, W., Boldrey, E., 1937. Somatic motor and sensory representation in the cerebral cortex of man as studied by electrical stimulation. *Brain* 60, 389-443, doi:DOI 10.1093/brain/60.4.389.

Plis, S.M., Hjelm, D.R., Salakhutdinov, R., Allen, E.A., Bockholt, H.J., Long, J.D., Johnson, H.J., Paulsen, J.S., Turner, J.A., Calhoun, V.D., 2014. Deep learning for neuroimaging: a validation study. *Front. Neurosci.* 8, 229, doi:10.3389/fnins.2014.00229.

Sermanet, P., Eigen, D., Zhang, X., Mathieu, M., Fergus, R., LeCun, Y., 2013. Overfeat: Integrated recognition, localization and detection using convolutional networks. arXiv preprint arXiv:1312.6229.

Sharif Razavian, A., Azizpour, H., Sullivan, J., Carlsson, S., 2014. CNN features off-the-shelf: an astounding baseline for recognition. *Proceedings of the IEEE conference on computer vision and pattern recognition workshops*, pp. 806-813.

Shirer, W.R., Ryali, S., Rykhlevskaia, E., Menon, V., Greicius, M.D., 2012. Decoding subject-driven cognitive states with whole-brain connectivity patterns. *Cereb. Cortex* 22, 158-165, doi:10.1093/cercor/bhr099.

Simonyan, K., Zisserman, A., 2014. Very deep convolutional networks for large-scale image recognition. arXiv preprint arXiv:1409.1556.

Smith, S.M., Jenkinson, M., Woolrich, M.W., Beckmann, C.F., Behrens, T.E.J., Johansen-Berg, H., Bannister, P.R., De Luca, M., Drobnjak, I., Flitney, D.E., Niazy, R.K., Saunders, J., Vickers, J., Zhang, Y.Y., De Stefano, N., Brady, J.M., Matthews, P.M., 2004. Advances in functional and structural MR image analysis and implementation as FSL. *NeuroImage* 23, S208-S219, doi:10.1016/j.neuroimage.2004.07.051.

Springenberg, J.T., Dosovitskiy, A., Brox, T., Riedmiller, M., 2014. Striving for simplicity: The all convolutional net. arXiv preprint arXiv:1412.6806.

Sulzer, J., Haller, S., Scharnowski, F., Weiskopf, N., Birbaumer, N., Blefari, M.L., Bruehl, A.B., Cohen, L.G., DeCharms, R.C., Gassert, R., Goebel, R., Herwig, U., LaConte, S., Linden, D., Luft, A., Seifritz, E., Sitaram, R., 2013. Real-time fMRI neurofeedback: progress and challenges. *NeuroImage* 76, 386-399, doi:10.1016/j.neuroimage.2013.03.033.

Tyndall, A.J., Reinhardt, J., Tronnier, V., Mariani, L., Stippich, C., 2017. Presurgical motor, somatosensory and language fMRI: Technical feasibility and limitations in 491 patients over 13 years. *Eur. Radiol.* 27, 267-278, doi:10.1007/s00330-016-4369-4.

Van Essen, D.C., Smith, S.M., Barch, D.M., Behrens, T.E., Yacoub, E., Ugurbil, K., Consortium, W.U.-M.H., 2013. The WU-Minn Human Connectome Project: an overview. *NeuroImage* 80, 62-79, doi:10.1016/j.neuroimage.2013.05.041.

Van Essen, D.C., Ugurbil, K., Auerbach, E., Barch, D., Behrens, T.E.J., Bucholz, R., Chang, A., Chen, L., Corbetta, M., Curtiss, S.W., Della Penna, S., Feinberg, D., Glasser, M.F., Harel, N., Heath, A.C., Larson-Prior, L., Marcus, D., Michalareas, G., Moeller, S., Oostenveld, R., Petersen, S.E., Prior, F., Schlaggar, B.L., Smith, S.M., Snyder, A.Z., Xu, J., Yacoub, E., Wu-Minn, H.C.P.C., 2012.

- The Human Connectome Project: A data acquisition perspective. *NeuroImage* 62, 2222-2231, doi:10.1016/j.neuroimage.2012.02.018.
- Vieira, S., Pinaya, W.H., Mechelli, A., 2017. Using deep learning to investigate the neuroimaging correlates of psychiatric and neurological disorders: Methods and applications. *Neurosci. Biobehav. Rev.* 74, 58-75, doi:10.1016/j.neubiorev.2017.01.002.
- Worsley, K.J., Friston, K.J., 1995. Analysis of fMRI time-series revisited--again. *NeuroImage* 2, 173-181, doi:10.1006/nimg.1995.1023.
- Yamins, D.L., DiCarlo, J.J., 2016. Using goal-driven deep learning models to understand sensory cortex. *Nat. Neurosci.* 19, 356-365, doi:10.1038/nn.4244.
- Yeh, C.-K., Wu, W.-C., Ko, W.-J., Wang, Y.-C.F., 2017. Learning Deep Latent Space for Multi-Label Classification. *AAAI*, pp. 2838-2844.
- Yosinski, J., Clune, J., Bengio, Y., Lipson, H., 2014. How transferable are features in deep neural networks? , *Adv. Neural Inf. Process. Syst.*, pp. 3320-3328.
- Zhang, W., Li, R., Deng, H., Wang, L., Lin, W., Ji, S., Shen, D., 2015. Deep convolutional neural networks for multi-modality isointense infant brain image segmentation. *NeuroImage* 108, 214-224, doi:10.1016/j.neuroimage.2014.12.061.